Reversible coordinative binding and separation of sulphur dioxide in a robust metal-organic framework with open copper sites

Gemma L. Smith,[1,a] Jennifer E. Eyley,[1,a] Xue Han,[1] Xinran Zhang[1], Jiangnan Li,[1] Nicholas M. Jacques,[1] Harry G.W. Godfrey,[1] Stephen P. Argent,[2] Laura J. M[c]Cormick,[3] Simon J. Teat,[3] Yongqiang Cheng,[4] Mark D. Frogley,[5] Gianfelice Cinque,[5] Sarah J. Day,[5] Chiu C. Tang,[5] Timothy L. Easun,[6] Svemir Rudić,[7] Anibal J. Ramirez-Cuesta,[4] Sihai Yang[1]* and Martin Schröder[1]*

1. School of Chemistry, University of Manchester, Manchester, M13 9PL (UK)

2. Department of Chemistry, University of Warwick, CV4 7AL (UK)

3. Advanced Light Source, Lawrence Berkeley National Laboratory, Berkeley, California 94720 (USA) 4. Oak Ridge National Laboratory, Oak Ridge, TN 37831(USA)

5. Diamond Light Source, Harwell Science Campus, Oxfordshire, OX11 0DE (UK)

6. School of Chemistry, Cardiff University, Cardiff, CF10 3AT (UK)

7. ISIS Facility, STFC Rutherford Appleton Laboratory, Chilton, Oxfordshire, OX11 0QX (UK)

a. these authors contributed equally to this work.

Emissions of sulphur dioxide (SO_2) from flue gas and marine transport have detrimental impacts on the environment and human health, but SO_2 is also an important industry feedstock if it can be recovered, stored and transported efficiently. Here we report the exceptional adsorption and separation of SO_2 in a porous material, $[Cu_2(L)]$ (H_4L = 4',4'''-(pyridine-3,5-diyl)bis([1,1'-biphenyl]-3,5-dicarboxylic acid), MFM-170. MFM-170 exhibits fully reversible SO_2 uptake of 17.5 mmol g^{-1} at 298 K, 1.0 bar, and the SO_2 binding domains for trapped molecules within MFM-170 have been determined. Significantly, we report reversible co-ordination of SO_2 to open Cu(II) sites in a porous material, contributing to excellent adsorption thermodynamics and selectivities for SO_2 binding, as well as facile regeneration of MFM-170 post adsorption. MFM-170 is stable to water, acid and base and shows significant promise for the dynamic separation of SO_2 from simulated flue gas mixtures, as confirmed by breakthrough experiments.

The use of fossil fuels is a major contributer to many serious environmental issues, but transition to clean energy sources remains challenging as new technologies mature. The release of SO_2, for which antrophogenic sources account for >87% of global emissions[1], has detrimental effects on the environment and human health but is also an important feedstock for sulphuric acid production. Furthermore, trace SO_2 can greatly reduce the activity of amine-based CO_2 scrubbers,[2] as well as irreversibly poisoning catalysts for selective NO_x reduction[3] and CH_4 combustion.[4]

In recent years, there has been growing interest in the development of dry regenerable sorbents for SO_2 operating under ambient conditions.[5-7] These materials offer advantages over existing wet flue gas desulphurisation (FDG) technologies by reducing energy and water requirements and minimising the generation of waste. Importantly, regeneration of sorbents allows recovery of saleable SO_2, which can be utilised further *via* conversion to elemental sulphur or sulfuric acid. High capacity sorbents for SO_2 can also be used for safe transportation of recovered gaseous SO_2 under ambient conditions, without the large energy demands required for pressurisation.

Porous metal-organic frameworks (MOFs) have been studied extensively for uptake and separation of a wide variety of gases, notably CO_2, H_2 and hydrocarbons,[9-14] but their application to SO_2 capture has been hindered by the toxic and highly corrosive nature of this substrate. To date, several MOFs have been tested as SO_2

adsorbents (Table 1, Fig 2),[15-25] but many exhibit limited stability and/or reversibility under near-ambient conditions. Current top-performing MOFs for SO_2 adsorption at 298 K and 1.0 bar include MFM-202a (10.2 mmol g^{-1})[18] and SIFSIX-1-Cu (11.0 mmol g^{-1})[16]. The former is subject to an irreversible phase change on SO_2 uptake, whilst the steep uptake of the latter may render it unfeasible for practical PSA applications.[26,27] As well low energy costs of system regeneration, sorbents for use in FGD processes require high SO_2/CO_2 selectivity at low partial pressures of SO_2 (~2000 ppm). Although open metal sites (OMSs) can improve gas binding selectivity, the resultant MOFs are often subject to framework degradation upon contact with water, precluding their practical applications.[28-31]

Herein, we report the first example of reversible coordinative binding of SO_2 to open Cu(II) sites in a remarkably robust material, MFM-170, leading to optimal adsorption and selectivity for SO_2. Coordination of the pyridyl N-donor to one axial site of the $Cu_2(O_2CR)_4$ paddlewheel unit leads to an unusual (3,36)-connected ***txt*** framework which, on removal of axial water, affords one open Cu(II) site per $Cu_2(O_2CR)_4$ paddlewheel in MFM-170. Significantly, at 298 K and 1.0 bar, MFM-170 exhibits an unprecedented uptake of SO_2 of 17.5 mmol g^{-1}, fully reversible at ambient temperature. We have unravelled the high selectivity of MFM-170 for SO_2 and have probed the nature of host-guest binding using *in situ* single crystal X-ray diffraction, FTIR micro-spectroscopy and neutron scattering. Importantly, breakthrough experiments of synthetic flue gas mixtures demonstrate that MFM-170 has excellent separation properties, even in the presence of water and at elevated temperatures. The stability of MFM-170 to wet SO_2 has been confirmed by long duration synchrotron X-ray diffraction experiments.

Synthesis and structural analysis of MFM-170·solv

Solvothermal reaction of a pyridine-containing tetracarboxylate linker 4',4'''-(pyridine-3,5-diyl)bis([1,1'-biphenyl]-3,5-dicarboxylic acid) (H_4L, Figs. 1a, S1**)** and $Cu(NO_3)_2 \bullet 2.5H_2O$ in a mixture of DMF and H_2O (v/v = 5:1) under acidic conditions (HNO_3) yielded blue octahedral crystals of $[Cu_2(L)(H_2O)] \bullet 6DMF$, denoted as MFM-170$\bullet H_2O \bullet$solv. Single crystal X-ray diffraction reveals that MFM-170$\bullet H_2O \bullet$solv crystallises in the cubic space group *Im-3m* to form a rarely observed (3,36)-connected net with ***txt*** topology (Figs. 1b-d).[32-34] The interconnected void spaces in MFM-170 can be considered as three distinct cages, denoted as ***A***, ***B*** and ***C*** (Fig. 1e). The metal-organic cuboctahedra (cage ***A***) have a dimension of 15.9 Å, comprised of alternating triangular and square faces. Each square face of cage ***A*** joins it to a cage ***B***, which is formed by four V-shaped linkers bowing outward to create a prolate pore (width of 16.3 Å; length of 22.2 Å). Cage ***C*** is the smallest of the three and connects

the triangular faces of cage ***A***, measuring 12.8 Å between opposite triangular faces, and 14.2 Å between opposite C atoms.

Thermal and chemical stability of MFM-170

Thermogravimetric analysis (TGA) of MFM-170•H_2O·solv shows thermal stability up to ~620 K, confirmed by variable temperature PXRD analysis (Figs. S4, S8). The chemical robustness of MFM-170•H_2O·solv to a range of harsh environmental conditions was investigated, including suspending the sample in boiling water and aqueous solutions of pH between 2-12. No loss in crystallinity was observed by PXRD after exposure to these conditions (Figs. 4b, S2, S3, S6). More importantly, desolvated MFM-170 can be re-hydrated to MFM-170·H_2O upon contact with water without loss of crystallinity. Reversible water adsorption isotherms are shown in Fig. S10. To assess the long-term stability of MFM-170 to humid SO_2 and water, synchrotron PXRD data were collected for wet SO_2-loaded MFM-170 samples every week for 10 weeks (Fig. S7; see SI for further details). No loss of crystallinity or change in the structure of this material was observed (Table S4), confirming the excellent chemical resilience of the framework, attributed to the unusual framework connectivity where the axially-coordinated pyridyl N-donors interlock the two cubic nets and block one of the two axial Cu(II) sites.

Analysis of gas adsorption isotherms of MFM-170 and MFM-170·H_2O

Desolvated MFM-170 possesses a BET surface area of 2408 $m^2\,g^{-1}$ (consistent with the calculated surface area of 2456 $m^2\,g^{-1}$ based upon the crystal structure) and a pore volume of 0.88 $cm^3\,g^{-1}$ (calculated from the N_2 isotherm at 77 K, Fig. S9), consistent with that (0.87 $cm^3\,g^{-1}$; solvent-accessible void space of 61%) derived from the single crystal structure. Significantly, MFM-170 shows an unprecedented SO_2 uptake of 19.4 mmol g^{-1} (or 1.24 g g^{-1}) at 273 K and 1.0 bar (Fig. 3). To the best of our knowledge, this represents the highest known SO_2 uptake capacity in porous materials, followed by MFM-601 (16.9 mmol g^{-1})[15], MFM-202a (13.0 mmol g^{-1})[18] and mesoporous silicate MCM-41 (11.6 mmol g^{-1})[35] under the same conditions. The performance of state-of-the-art porous materials under ambient conditions is summarised in Table 1 and Fig. 2. MFM-170 exhibits the highest reported SO_2 adsorption capacity of 17.5 mmol g^{-1} at 298 K and 1.0 bar, notably exceeding the current leading MOFs, such as MFM-601 (12.3 mmol g^{-1})[15], SIFSIX-1-Cu (11.0 mmol g^{-1})[16], [$Zn_2(L_1)_2$(bipy)] (10.9 mmol g^{-1}, at 293 K),[17] and Ni(bdc)$(ted)_{0.5}$ (10.0 mmol g^{-1}).[19] Furthermore, MFM-170 shows high SO_2 adsorption at elevated temperatures (11.6 mmol g^{-1} at 333 K and 1 bar; Fig. 3b). Uptake of SO_2 in MFM-170 shows a reversible type I isotherm with high uptakes at low pressure (Fig. 3); at 273 K the uptake at 0.03 bar is 6.5 mmol g^{-1}. Despite the high uptake at low pressure, the excellent reversibility of the SO_2 isotherms at 273-333 K indicates that MFM-170 can be fully regenerated under pressure-swing conditions. More significantly,

no loss of adsorption capacity of SO_2 was detected in MFM-170 after 50 adsorption-desorption cycles at 298 K (Fig. 4a), and PXRD analysis of MFM-170 after these 50 cycles confirms the full retention of crystal structure, reflecting the exceptional chemical and thermal stability of this material (Fig. 4b).

To probe the effect of the OMSs on SO_2 uptake, isotherms were measured for the coordinatively saturated parent material, MFM-170•H_2O, in which the axial water molecule is retained on the Cu(II) site. The SO_2 isotherm of MFM-170•H_2O at 273 K shows a reduced but still exceptionally high uptake of SO_2 (16.2 mmol g^{-1}) (Fig. S15). The difference in adsorption at 1.0 bar between MFM-170•H_2O and MFM-170 corresponds to approximately twice the density of open Cu(II) sites (1.46 mmol g^{-1}), suggesting that the presence of OMSs has a key role in promoting the SO_2 uptake.

In comparison to the high SO_2 uptake at 298 K and 1 bar, MFM-170 uptakes only 3.04 mmol g^{-1} of CO_2, 1.33 mmol g^{-1} of CH_4, 0.38 mmol g^{-1} of CO and 0.28 mmol g^{-1} of N_2 under the same conditions (Figs. 3a, S11-14). The selectivity values of MFM-170 for SO_2/CO_2, SO_2/N_2, SO_2/CO and SO_2/CH_4 were calculated from single component isotherms at 298 K (Figs. S19, S20). Due to the negligible interaction of N_2 with the framework, MFM-170 exhibits a high IAST selectivity of 944 for an equimolar mixture of SO_2/N_2 at 1.0 bar. Furthermore, MFM-170 also has high selectivity values of 260, 203 and 35 for SO_2/CH_4, SO_2/CO and SO_2/CO_2, respectively. More importantly and considering the relatively low concentrations of SO_2 present in flue gas, decreasing the SO_2:X ratio from 50:50 to 1:99 still affords high selectivity values for SO_2/N_2 (260) and SO_2/CO_2 (28). These values are lower than those reported for SIFSIX-2-Cu-i,[16] which possesses much narrower pores than MFM-170.

Determination of the binding domains for adsorbed SO_2 molecules in MFM-170 and MFM-170·H_2O

The binding domains of SO_2 were studied using *in situ* synchrotron X-ray single crystal diffraction. Structural analysis of desolvated MFM-170 confirms the complete removal of free solvents in the pore and bound water molecules on the Cu(II) sites, generating twelve open Cu(II) sites on the internal surface of cage ***A*** in desolvated MFM-170. Refinement of the diffraction data for the SO_2-loaded sample at 298 K revealed significant residual electron densities which were sequentially assigned as six distinct binding sites (**1-6**) in order of decreasing occupancy, giving a formula of $[Cu_2(L)(SO_2)_{0.67}](SO_2)_{4.79}$ (denoted as MFM-170•5.46SO_2) (Fig. 5).

The primary binding site, **1**, is situated on a three-fold rotational axis in the triangular window of cage ***A*** and has full occupancy (Fig. 5b). The S_{SO_2} atom points towards the $Cu_2(O_2CR)_4$ paddlewheel, forming close contacts with two carboxylate O

centers [$S_{so2}(\delta^+)\bullet\bullet\bullet(\delta^-)O$ =3.16(3) Å]. Simultaneously, the O_{so2} atom located in the centre of the window forms a three-fold supplementary interaction to the isophthalate C-H groups lining the window [$O_{so2}\bullet\bullet\bullet C$ =4.18(3) Å, <O•••H-C =140.5(6)°]. SO_2(**2**) is coordinated to the open Cu(II) site in an end-on manner [O_{so2}-Cu =2.28(10) Å] with an occupancy of 0.67. The O_{so2}-Cu bond distance is shorter than the sum of van der Waals radius of Cu and O (2.92 Å), confirming the formation of a covalent bond. The two O_{so2} atoms are parallel to the Cu•••Cu axis, whilst the S_{so2} is disordered about a C_2 axis. Significantly, this is the first crystallographic example of SO_2 coordination at OMSs within a MOF structure. Remarkably, the Cu(II) center is not the most occupied site, which is at least in part due to steric hindrance created by site **1**; the twelve Cu(II) sites line the internal surface of cage ***A*** and are therefore accessed through the square faces as the triangular windows are fully occupied by SO_2 molecules.

SO_2(**3**) (occupancy =0.47) is located in a crevice between cage ***B*** of one net and a perpendicular cage ***B*** of the second net (Fig. 5b). This small pocket accommodates interactions with the face of the pyridine ring [$S_{so2}\bullet\bullet\bullet N$ =3.48(18) Å] and phenyl H atoms [$O_{so2}\bullet\bullet\bullet C^4$ =3.20(4) Å, $O_{so2}\bullet\bullet\bullet C^{11}$ =4.80(4) Å], accounting for ~30% of all located SO_2 molecules. SO_2(**4**) (occupancy =0.32), is found in cage ***C*** and situated with the S atom facing the carboxylate oxygens of the paddlewheel [$S_{so2}(\delta^+)\bullet\bullet\bullet(\delta^-)O^1$ =3.67(3) Å] and interacts with neighbouring phenyl rings [$O_{so2}\bullet\bullet\bullet C^7$ = 3.70(5) Å, $O_{so2}\bullet\bullet\bullet$ring centroid =3.26(5) Å]. SO_2(**5**) is found in the square face between cages ***A*** and ***B*** with an occupancy of 0.26. Whilst no significant interaction with the framework was identified, dipole interactions between the adsorbed SO_2 molecules were observed [S_{so2}**(2)**$\bullet\bullet\bullet O_{so2}$**(5)** =2.54(6) Å, O_{so2}**(5)**$\bullet\bullet\bullet S_{so2}$**(6)**=2.88(5) Å]. The least populated site (**6**) (occupancy = 0.23) is sandwiched between two phenyl rings in cage ***C*** and forms interactions between the S(δ^+) and the phenyl π-electrons at distances of 3.28(15) and 3.30(15) Å, measured between the ring centroids and S_{so2}.

We sought to examine the most thermodynamically favoured site *via* controlled desorption of MFM-170•5.46SO_2. Crucially, diffraction data collected for the sample under dynamic vacuum at 298 K showed that almost all adsorbed SO_2 molecules were removed from the structure of MFM-170, leaving just the Cu(II)-bound SO_2(**2**) with an occupancy of 0.09. This confirms that the Cu(II) site is indeed the thermodynamically strongest binding site but is sufficiently weak to be almost entirely desorbed on reduction of pressure. Interestingly, DFT calculations indicated that for MOF-74(M) (M = Mg, Ni, Co, Zn), the sites with highest binding energies for SO_2 were located at the

OMSs.[37] For MFM-170 the multi-site cooperative binding between SO_2 molecules (Fig. 5c) results in an optimal balance of high selectivity and excellent reversibility of the SO_2 adsorption that is observed. Subsequent brief heating to 400 K fully regenerated MFM-170 without any loss of crystallinity.

To investigate the nature of SO_2 binding in the absence of OMSs, a single crystal of MFM-170•H_2O·solv was activated under mild conditions to remove free solvent molecules whilst leaving the axial water molecule bound to the Cu centre. The resultant MFM-170•H_2O was loaded with 1 bar SO_2 and subsequent refinement of the diffraction data gave a structure with formula of $[Cu_2(L)(H_2O)_{0.79}](SO_2)_{3.27}$ (denoted MFM-170•H_2O•3.27SO_2). Significantly, of the six SO_2 molecules previously located in MFM-170•5.46SO_2, four are also present in MFM-170•H_2O•3.27SO_2 (Fig. S26). Clearly, the site Cu(II)-bound SO_2(**2**) was absent in MFM-170•H_2O•3.27SO_2, and as SO_2(**2**) is a primary site of interaction for SO_2(**5**), the latter was not located either. However, overall the structural analysis shows that saturation of the copper sites in MFM-170 with H_2O does not greatly reduce the SO_2 binding capacity, consistent with the retention of high uptake capacity in MFM-170•H_2O.

In situ spectroscopic analysis of host-guest binding dynamics

In situ FTIR spectroscopic studies were conducted for MFM-170 as a function of SO_2 loading (Figs. 6a-c). The growth of a new peak at 1143 cm^{-1} (Fig. 6c) was assigned to the ν_1 symmetric stretch of adsorbed SO_2, which increases as a function of SO_2 partial pressure (pp). This symmetric band is red-shifted from 1152 cm^{-1} (Δ = -9 cm^{-1}) for free SO_2, confirming its interaction with the framework. A second new band, assigned to the ν_3 asymmetric stretch of adsorbed SO_2, grows and red-shifts from 1340 cm^{-1} at 0.01 ppSO_2 to 1320 cm^{-1} at 0.10 ppSO_2 (Fig. 6b). These bands show larger shifts compared to gas phase SO_2 (Δ= -41 cm^{-1} at 0.10 ppSO_2), but are consistent with physisorption of SO_2.[36-38]

Significant vibrational changes of the framework were also observed on SO_2 adsorption. The carboxylate ν_{as}(COO) mode at 1658 cm^{-1} (Fig. 6a) and ν_s(COO) mode at 1470 cm^{-1} (Fig. 6b) of MFM-170 decrease in intensity and are red-shifted to 1648 cm^{-1} (Δ = -10 cm^{-1}) and 1462 cm^{-1} (Δ = -8 cm^{-1}) at 0.50 ppSO_2, respectively. Interestingly, this is distinct from the blue-shifts of these bands observed in previously reported MOFs on SO_2 loading.[19] This is likely due to the lack of OMSs in those reported structures, and therefore is consistent with interactions of SO_2 with the Cu site in MFM-170. Furthermore, a red-shift (Δ = -16 cm^{-1}) of the band at 1595 cm^{-1} on SO_2 binding, assigned to the pyridine ring vibrational band ν(CC/CN), suggests a weakening of the pyridine N-Cu coordination on SO_2 adsorption.[39]

In situ INS experiments were conducted for dry and wet MFM-170 to gain further insight into the dynamics of SO_2 binding (Figs. 6d-f, S22-24). Comparison of the spectra of bare MFM-170 and MFM-170•H_2O allows clear assignment of the water modes (Fig. 6d). The peak observed at 8.3 meV in the bare MOF can be attributed to a lattice mode which, on SO_2 loading, increases in intensity and shifts to 9.2 meV, suggesting a stiffening effect in MFM-170 on SO_2 binding (Fig. 6e). Overall, there is lack of change to the INS features upon SO_2 adsorption in MFM-170, indicating a moderate-to-weak host-guest interaction, fully consistent with the high stability and ease of regeneration. Upon SO_2 loading of MFM-170•H_2O, notable spectral changes are observed, attributed to interactions between bound water and SO_2 molecules (Fig. 6f). The broad translational band at 30 meV increases in intensity, whilst the water rocking mode increases in intensity with a blue-shift from 48 to 49 meV. The librational mode at 66 meV also blue-shifts to 67 meV with a decrease in intensity. Importantly, subsequent activation of the SO_2-adsorbed MFM-170•H_2O at 373 K under vacuum removed all peaks assigned to water, and led to a spectrum consistent with the dry bare MOF, further evidencing the stability of the MOF to humid SO_2 (Fig. S22).

Dynamic breakthrough separation of SO_2 in MFM-170. To test the effect of humidity on SO_2 adsorption in MFM-170, dynamic breakthrough experiments were conducted using either dry or wet synthetic flue gas mixtures (Fig. 3c). Under dry conditions, SO_2 begins to breakthrough at dimensionless time τ = 420 and reaches a maximum by τ = 1400. With the addition of 1.5% water, MFM-170 exhibits a slightly reduced SO_2 retention time at τ = 370. Importantly, three cycles of SO_2 breakthrough and desorption (Fig. 3c) confirmed no significant deterioration in performance. To investigate further the separation ability for SO_2/CO_2, breakthrough experiments were also carried out using simulated flue gas mixtures for a fully-activated sample and a water-saturated sample of MFM-170 (Fig. 3d). For the dry sample, the breakthrough curve at 298 K shows that CO_2 is the first component eluted through the fixed-bed packed of MFM-170 and breaks through at dimensionless time τ =14. In comparison, SO_2 was selectively retained by MFM-170 and breaks through much later (τ =~350) with maximum output observed by τ =1450. After the breakthrough of SO_2, the packed bed was regenerated at 298 K by flowing pure helium through it, and this results in rapid desorption of both CO_2 and SO_2. No more SO_2 was detected in the effluent stream when the temperature was subsequently increased to 423 K, indicating the complete regeneration of MFM-170 at 298 K. Crucially, the ability of MFM-170 to separate SO_2 from CO_2 in the presence of a large quantity of water was confirmed by repeating the breakthrough experiments with a water-saturated fixed-bed. The column was exposed to a stream of 3% H_2O in He until breakthrough and saturation of water was observed. The subsequent breakthrough experiment

demonstrated excellent SO_2/CO_2 separation under these conditions (Fig. 3d). Interestingly, whilst the breakthrough times were slightly decreased for both components than in the above experiments, CO_2 is affected more severely with a much steeper breakthrough. Unlike the dry sample, a significant roll-up effect is observed for CO_2 under humid conditions, indicating a large displacement of weakly bound CO_2 by SO_2, likely due to the formation of H_2SO_3 complexes in the pore. This suggests that the SO_2/CO_2 separation in MFM-170 could be enhanced under humid conditions. Breakthrough experiments were also conducted for activated MFM-170 at elevated temperatures of 323 and 348 K (Fig. S25), to test suggested suitable temperatures ranges for FGD.[2,3] Importantly, a very clear separation between CO_2 and SO_2 is evident at both temperatures, though, as expected, with reduced retention time.

Outlook

The development of efficient strategies to fully mitigate emissions of SO_2 from combustion and to achieve efficient SO_2 storage and safe transport remains a fundamental challenge for many industries, power-plants and marine transport sectors. Although emerging MOF materials show great promise as sorbents for a wide range of inert gases, relatively little success has been achieved on the adsorptive removal of SO_2, primarily due to the generally limited reversibility and/or stability of MOFs upon contact with highly corrosive SO_2. The present work describes a high SO_2 uptake of 17.5 mmol g^{-1} at ambient conditions in a remarkably stable MOF with open Cu(II) sites with high selectivity for SO_2 over CO_2 and N_2. The binding sites of SO_2 in MFM-170 have been elucidated using *in situ* single crystal diffraction which revealed the reversible coordination of SO_2 at open Cu(II) sites and five other binding sites at crystallographic resolution. Crucially, the open Cu(II) site has been identified as the most thermodynamically favoured binding site for SO_2. In addition to static crystallography studies, dynamic vibrational modes were investigated using INS and FT-IR microscopy as a function of SO_2 loading. The industrial promise of MFM-170 has been demonstrated through dynamic breakthrough experiments which showed efficient separation of SO_2 from simulated flue gas mixtures, even in the presence of water and at elevated temperatures.

References

1. Rezaei, F. *et al.* SO_x/NO_x Removal from flue gas streams by solid adsorbents: a review of current challenges and future directions. *Energy & Fuels* **29**, 5467–5486 (2015).

2. Gao, J. *et al* Pilot-scale experimental study on the CO_2 capture process with existing of SO_2: degradation, reaction rate, and mass transfer. *Energy & Fuels* **25**, 5802–5809 (2011).
3. Ding, S. *et al.* Significant promotion effect of Mo additive on a novel Ce–Zr mixed oxide catalyst for the selective catalytic reduction of NO_x with NH_3. *ACS Appl. Mater. Interfaces* **7**, 9497–9506 (2015).
4. Kinnunen, N. M. *et al.* Case study of a modern lean-burn methane combustion catalyst for automotive applications: What are the deactivation and regeneration mechanisms? *Appl. Catal. B Environ.* **207**, 114–119 (2017).
5. Han, X., Yang, S., Schröder, M. Porous metal–organic frameworks as emerging sorbents for clean air. *Nat. Rev. Chem.*, **3**, 108–118 (2019).
6. Raymundo-Piñero, E. *et al.* Factors controling the SO_2 removal by porous carbons: relevance of the SO_2 oxidation step. *Carbon*, **38**, 335–344 (2000).
7. Mathieu, Y. *et al.* Adsorption of SO_x by oxide materials: A review. *Fuel Process. Technol.* **114,** 81–100 (2013).
8. Kohl, A. L. & Nielsen, R. *Gas Purification*. (Gulf Professional Publishing, 1997).
9. Nabais, A. R. *et al.* CO_2/N_2 gas separation using Fe(BTC)-based mixed matrix membranes: a view on the adsorptive and filler properties of metal-organic frameworks. *Sep. Purif. Technol.* **202**, 174–184 (2018).
10. Peng, J. *et al.* Efficient kinetic separation of propene and propane using two microporous metal organic frameworks. *Chem. Commun.* **53**, 9332–9335 (2017).
11. Chen, D.-M. *et al.* Tunable robust pacs-MOFs: a platform for systematic enhancement of the C_2H_2 uptake and C_2H_2/ C_2H_4 separation performance. *Inorg. Chem.* **57**, 2883–2889 (2018).
12. Zhong, R. *et al.* A solvent ‘squeezing’ strategy to graft ethylenediamine on $Cu_3(BTC)_2$ for highly efficient CO_2/CO separation. *Chem. Eng. Sci.* **184**, 85–92 (2018).
13. Zhang, Z. *et al.* MOFs for CO_2 capture and separation from flue gas mixtures: the effect of multifunctional sites on their adsorption capacity and selectivity. *Chem. Commun.* **49**, 653–661 (2013).
14. Peralta, D. *et al.* Comparison of the behavior of metal–organic frameworks and zeolites for hydrocarbon separations. *J. Am. Chem. Soc.* **134**, 8115–8126 (2012).
15. Carter, J. H. *et al.* Exceptional adsorption and binding of sulfur dioxide in a robust zirconium-based metal–organic framework. *J. Am. Chem. Soc.* **140,** 15564–15567 (2018).
16. Cui, X. *et al.* Ultrahigh and selective SO_2 uptake in inorganic anion-pillared hybrid porous materials. *Adv. Mater.* **29**, 1606929 (2017).

17. Glomb, S. *et al*. Metal–organic frameworks with internal urea-functionalized dicarboxylate linkers for SO_2 and NH_3 adsorption. *ACS Appl. Mater. Interfaces* **9**, 37419–37434 (2017).
18. Yang, S. *et al.* Irreversible network transformation in a dynamic porous host catalyzed by sulfur dioxide. *J. Am. Chem. Soc.* **135**, 4954–4957 (2013).
19. Tan, K. *et al.* Mechanism of preferential adsorption of SO_2 into two microporous paddle wheel frameworks $M(bdc)(ted)_{0.5}$. *Chem. Mater.* **25**, 4653−4662 (2013).
20. Savage, M. *et al.* Selective adsorption of sulfur dioxide in a robust metal-organic framework material. *Adv. Mater.* **28**, 8705–8711 (2016).
21. Li, L. *et al.* Post-synthetic modulation of the charge distribution in a metal–organic framework for optimal binding of carbon dioxide and sulfur dioxide. *Chem. Sci.* **10,** 1472–1482 (2019).
22. Lee, G.-Y. *et al.* Amine-functionalized covalent organic framework for efficient SO_2 capture with high reversibility. *Sci. Rep.* **7**, 557 (2017).
23. Thallapally, P. K. *et al*. Prussian blue analogues for CO_2 and SO_2 capture and separation applications. *Inorg. Chem.* **49**, 4909–4915 (2010).
24. Fernandez, C. *et al.* Gas-induced expansion and contraction of a fluorinated metal−organic framework. *Cryst. Growth Des.* **10**, 1037–1039 (2010).
25. Tchalala, M. R. *et al.* Fluorinated MOF platform for selective removal and sensing of SO_2 from flue gas and air. *Nat. Commun.* **10,** 1328 (2019).
26. Riboldi, L. & Bolland, O. Overview on pressure swing adsorption (PSA) as CO_2 capture technology: state-of-the-art, limits and potentials. *Energy Procedia* **114,** 2390–2400 (2017).
27. Riboldi, L. & Bolland, O. Evaluating pressure swing adsorption as a CO_2 separation technique in coal-fired power plants. *Int. J. Greenh. Gas Control* **39,** 1–16 (2015).
28. Britt, D. *et al.* Highly efficient separation of carbon dioxide by a metal-organic framework replete with open metal sites. *Proc. Natl. Acad. Sci.* **106**, 20637–20640 (2009).
29. Wong-Foy, A. G., Matzger, A. J. & Yaghi, O. M. Exceptional H_2 saturation uptake in microporous metal−organic frameworks. *J. Am. Chem. Soc.* **128**, 3494–3495 (2006).
30. Caskey, S. R., Wong-Foy, A. G. & Matzger, A. J. Dramatic tuning of carbon dioxide uptake via metal substitution in a coordination polymer with cylindrical pores. *J. Am. Chem. Soc.* **130**, 10870–10871 (2008).
31. Britt, D., Tranchemontagne, D. & Yaghi, O. M. Metal-organic frameworks with high capacity and selectivity for harmful gases. *Proc. Natl. Acad. Sci.* **105**, 11623–11627 (2008).

32. Guillerm, V. *et al.* A supermolecular building approach for the design and construction of metal–organic frameworks. *Chem. Soc. Rev.* **43**, 6141–6172 (2014).
33. Park, J. *et al.* A versatile metal–organic framework for carbon dioxide capture and cooperative catalysis. *Chem. Commun.* **48**, 9995-9997 (2012).
34. Lu, Z. *et al.* The utilization of amide groups to expand and functionalize metal-organic frameworks simultaneously. *Chem. - A Eur. J.* **22**, 6277–6285 (2016).
35. Branton, P. J., Hall, P. G., Treguer, M. & Sing, K. S. W. Adsorption of carbon dioxide, sulfur dioxide and water vapour by MCM-41, a model mesoporous adsorbent. *J. Chem. Soc., Faraday Trans.* **91**, 2041–2043 (1995).
36. Goodman, A. L., Li, P., Usher, C. R. & Grassian, V. H. Heterogeneous uptake of sulfur dioxide on aluminum and magnesium oxide particles. *J. Phys. Chem. A* **105**, 6109–6120 (2001).
37. Tan, K. *et al.* Interaction of acid gases SO_2 and NO_2 with coordinatively unsaturated metal organic frameworks: MOF-74 (M = Zn, Mg, Ni, Co). *Chem. Mater.* **29**, 4227-4235 (2017).
38. Schneider, W. F., Li, J. & Hass, K. C. Combined computational and experimental investigation of SO_x adsorption on MgO. *J. Phys. Chem. B* **105**, 6972–6979 (2001).
39. Marinho, M. V. *et al.* Synthesis, crystal structure, and spectroscopic characterization of trans-bis[(μ-1,3-bis(4-pyridyl)propane)(μ-(3-thiopheneacetate-*O*))(3-thiopheneacetate-*O*)]dicopper(II), $\{[Cu_2(O_2CCH_2C_4H_3S)_4\ \mu\text{-}(BPP)_2]\}_n$: from a dinuclear paddle-wheel copper(II) unit to a 2-D coordination polymer involving monatomic carboxylate bridges. *Inorg. Chem.* **43**, 1539–1544 (2004).

Methods

SO_2 safety: All systems involved in the supply, delivery and measurement of SO_2 were rigorously leak tested and used only within range of a SO_2 detection system with a sensitivity of 0.1 ppm. All gases exhausted from experimental apparatus were diluted with a flow of N_2 and fed into fume hood extracts.

Synthesis of MFM-170·solv: $[Cu_2(C_{33}H_{17}NO_8)(H_2O)]\bullet 6(C_3H_7NO)$**:** H_4L (192 mg, 0.36 mmol) and $Cu(NO_3)_2{\cdot}2.5H_2O$ (298 mg, 1.28 mmol) were dissolved in a solution of DMF:H_2O (48 mL, 5:1) and acidified with conc. HNO_3 (0.3 mL). The solution was heated in a Schott bottle at 80°C for 18 h until blue octahedral crystals precipitated. The product was filtered, washed with hot DMF and dried in air (320 mg, 86%). IR (ATR) cm^{-1}: 3382 (b), 1698 (w), 1645 (s), 1598 (s), 1557 (s), 1428 (s), 1378 (vs), 1298 (s),

1244 (w), 1170 (w), 1116 (m). Elemental analysis (% calculated/found): C 53.46/52.93; H 4.89/4.61; N 6.93/7.18. Powder samples of MFM-170·H_2O•solv in this work were obtained by stirring identical reaction mixtures in an open round bottom flask. Pawley refinement of the bulk powder sample of MFM-170 is shown in Fig. S5. Whilst the sum formula from single crystal X-ray diffraction included in the refinement model is $Cu_2(C_{33}H_{17}NO_8)(H_2O)_{0.65}$, the final formula of $[Cu_2(C_{33}H_{17}NO_8)(H_2O)]$•$6(C_3H_7NO)$ was calculated from a combination of TGA and elemental analysis, accounting for disordered solvent molecules.

Gas Cell Details and Structure Determination and Refinement of MFM-170·H_2O·solv, MFM-170, MFM-170·5.46SO_2, MFM-170·0.09SO_2, MFM-170·H_2O and MFM-170·H_2O·3.27SO_2

Gas-loaded single crystal X-ray diffraction experiments of MFM-170 were carried out at beamline 11.3.1 of the Advanced Light Source, Berkeley. Single crystals of MFM-170 were placed in a capillary gas handling cell and were evacuated *in situ* under a hot stream of N_2 centred on the capillary. The activated crystals were then cooled to *ca.* 300 K before being dosed with 1 bar of SO_2. The locations of the SO_2 molecules could be discerned from the Fourier difference maps at 300 K (MFM-170•5.46SO_2, MFM-170•0.09SO_2) and 260 K (MFM-170•H_2O•3.27SO_2) and were included in the refinement model with bond distances and angles constrained to ideal values. See Supplementary Information for details of structure determination and refinement.

Crystal Data for MFM-170·H_2O·solv $[Cu_2(C_{33}H_{17}NO_8)(H_2O)_{0.65}]$; blue octahedron (0.1 x 0.1 x 0.1 mm). Cubic, *Im-3m*, a = 33.5294(17) Å, V = 37963(7) Å, Z = 24, ρ_{calcd} = 0.729 g cm^{-1}. μ_{calcd} = 0.883 mm^{-1}, F(000) = 8413. A total of 45304 reflections were collected, of which 1475 were unique giving R int = 0.153. Final R_1 (wR_2) = 0.0465 (0.1226) with GoF = 1.130. The final difference Fourier extreme were 0.427 and -0.568 e$Å^{-3}$.

Crystal Data for desolvated MFM-170 $[Cu_2(C_{33}H_{17}NO_8)]$; purple octahedron (0.1 x 0.1 x 0.1 mm). Cubic, *Im-3m*, a = 33.609(2) Å, V = 37694(6) Å, Z = 24, ρ_{calcd} = 0.722 g cm^{-1}. μ_{calcd} = 0.883 mm^{-1}, F(000) = 8256. A total of 42452 reflections were collected, of which 1043 were unique giving R int = 0.197. Final R_1 (wR_2) = 0.039 (0.097) with GoF = 1.045. The final difference Fourier extreme were 0.320 and -0.381 e$Å^{-3}$.

Crystal Data for MFM-170·5.46SO_2 $[Cu_2(C_{33}H_{17}NO_8)(SO_2)_{0.67}](SO_2)_{4.79}$; blue octahedron (0.1 x 0.1 x 0.1 mm). Cubic, *Im-3m*, a =33.5808(17) Å, V = 37868(6) Å, Z = 24, ρ_{calcd} = 1.086 g cm^{-1}. μ_{calcd} = 1.144 mm^{-1}, F(000) = 12448. A total of 105823 reflections were collected, of which 2202 were unique giving R int = 0.186. Final R_1

(wR_2) = 0.117 (0.331) with GoF = 1.663. The final difference Fourier extreme were 1.577 and -1.156 eÅ^{-3}.

Crystal Data for MFM-170·0.09SO$_2$ [$Cu_2(C_{33}H_{17}NO_8)(SO_2)_{0.09}$]; blue octahedron (0.1 x 0.1 x 0.1 mm). Cubic, *Im-3m*, a =33.5458(19) Å, V = 37750(6) Å, Z = 24, ρ_{calcd} = 0.727 g cm^{-1}. μ_{calcd} = 0.890 mm^{-1}, F(000) = 8324. A total of 73416 reflections were collected, of which 1471 were unique giving R int = 0.173. Final R_1 (wR_2) = 0.0411 (0.092) with GoF = 1.083. The final difference Fourier extreme were 0.517 and -0.474 eÅ^{-3}.

Crystal Data for MFM-170·H$_2$O [$Cu_2(C_{33}H_{17}NO_8)(H_2O)_{0.50}$]; blue octahedron (0.1 x 0.1 x 0.1 mm). Cubic, *Im-3m*, a =33.4562(16) Å, V = 37448(5) Å, Z = 24, ρ_{calcd} = 0.736 g cm^{-1}. μ_{calcd} = 0.895 mm^{-1}, F(000) = 8376. A total of 110623 reflections were collected, of which 2211 were unique giving R int = 0.0699. Final R_1 (wR_2) = 0.0565 (0.1799) with GoF = 1.124. The final difference Fourier extreme were 0.702 and -0.458 eÅ^{-3}.

Crystal Data for MFM-170·H$_2$O·3.27SO$_2$ [$Cu_2(C_{33}H_{17}NO_8)(H_2O)_{0.79}](SO_2)_{3.27}$; blue octahedron (0.1 x 0.1 x 0.1 mm). Cubic, *Im-3m*, a =33.610(4)) Å, V = 37968(12) Å^3, Z = 24, ρ_{calcd} = 0.951 g cm^{-1}. μ_{calcd} = 1.039 mm^{-1}, F(000) = 10957. A total of 84668 reflections were collected, of which 1720 were unique giving R int = 0.078. Final R_1 (wR_2) = 0.0947 (0.3006) with GoF = 1.529. The final difference Fourier extreme were 0.909 and -0.618 eÅ^{-3}.

A more detailed description of single crystal X-ray diffraction data can be found in the supplementary information.

Gas adsorption isotherms and breakthrough experiment: Measurements of SO_2 adsorption isotherms (0–1 bar) were performed using a Xemis gravimetric adsorption apparatus (Hiden Isochema, Warrington, UK) equipped with a clean ultrahigh vacuum system. The pressure in the system is accurately regulated by mass flow controllers. Research grade SO_2 and He were purchased from AIRLIQUIDE or BOC and used as received. In a typical gas adsorption experiment, 70-100 mg of MFM-170•H_2O·solv was loaded into the Xemis, and degassed at 423 K and high dynamic vacuum (10^{-10} bar) for 1 day to give desolvated MFM-170. Calculated heats of adsorption (Q_{st}) are shown in Figs. S16-18.

Breakthrough experiments were carried out in a 7 mm diameter fixed-bed tube of 120 mm length packed with 1.5 g of MFM-170 powder (particle size < 5 microns). The total volume of the bed was *ca*. 5 cm^3. The sample was heated at 423 K under a flow of He for 2 days for complete activation. The fixed-bed was then cooled to room temperature (298 K) using a temperature programmed water bath and the breakthrough experiment was performed with streams of SO_2 (0.5% diluted in He) and

CO_2 at atmospheric pressure and room temperature. The flow rate of the entering gas mixture was maintained at 47 mL min^{-1}, and the gas concentration, C, of SO_2 and CO_2 at the outlet determined by mass spectrometry and compared with the corresponding inlet concentration C_0, where $C/C_0 = 1$ indicates complete breakthrough. A more detailed description is given in SI.

Data Availability

Results of the refinements of the solvated, evacuated and SO_2-loaded crystal structures of MFM-170 have been deposited as CIF files as CCDC numbers 1538125-1538126, 1538129 and 1853512-1853514. These data can be obtained free of charge via https://www.ccdc.cam.ac.uk/structures/.

Supplementary Information is available in the online version of the paper.

Acknowledgements. We thank EPSRC (EP/I011870), ERC (AdG 742041), the Royal Society and University of Manchester for funding. We are especially grateful to Diamond Light Source (DLS), Advanced Light Source, Oak Ridge National Laboratory and STFC/ISIS Neutron Facility for access to the Beamlines B22/I11, 11.3.1, VISION and TOSCA, respectively. We thank Mark Kibble for the help at TOSCA beamline. The computing resources were made available through the VirtuES and the ICE-MAN projects, funded by Laboratory Directed Research and Development program at ORNL. This research used resources of the Advanced Light Source, which is a DOE Office of Science User Facility under contract no. DE-AC02-05CH11231. JL, XZ thank China Scholarship Council for funding.

Author Contributions. GLS, JEE: synthesis and characterisation of MOF samples, measurements of adsorption isotherms. GLS, XH: measurements and analysis of the breakthrough data. GLS, XZ, SPA, LJM, SJT, SY: collection and analysis of synchrotron single crystal X-ray diffraction data. GLS, HGWG, YC, SR, AJRC: collection and analysis of neutron scattering data. GLS, SJD and CCT: collection and analysis of long duration synchrotron X-ray diffraction data. GLS, JL, NMJ, MDF, GC, TLE: collection and analysis of synchrotron IR data. SY and MS: overall design and direction of project. GLS, SY and MS: preparation of the manuscript with help from all authors.

Author Information. The crystal structures are available free of charge from the Cambridge Crystallographic Data Centre under reference number CCDC-1538125-6, 1538129, 1853512-4. Reprints and permissions information is available at

www.nature.com/reprints. The authors declare no competing financial interests. Correspondence and requests for materials should be addressed to S.Y. (Sihai.Yang@manchester.ac.uk) and M.S. (M.Schroder@manchester.ac.uk).

Competing financial interests. The authors declare no competing financial interests.

Data availability. All relevant data are available from the authors, and/or are included with the manuscript.

Figures and Tables

a) b)

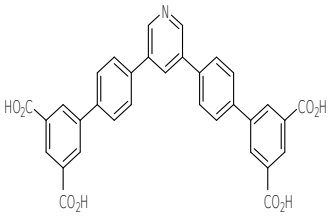

H_4L

c) d)

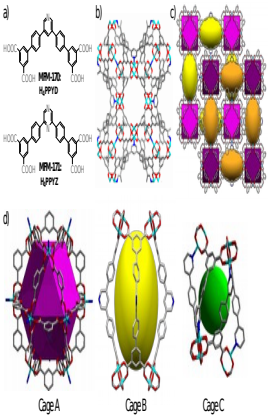

e)

16.3 Å

12.8 Å

15.9 Å

22.2 Å

Cage ***A*** Cage ***B*** Cage ***C***

Fig. 1: Structure of MFM-170 solved from single crystal X-ray data. The metal cluster of MFM-170 consists of a $Cu_2(O_2CR)_4$ paddlewheel with four isophthalate units occupying the equatorial sites and one pyridyl N-donor from the ligand coordinating to the axial site of one Cu atom. The axial position of the other Cu atom of the $Cu_2(O_2CR)_4$ unit is occupied by a water molecule. The framework is constructed from $Cu_{24}(RC_6H_3(CO_2)_2)_{24}$ cuboctahedron, which acts as a 36-connected node, joined in a cubic array to six adjacent cuboctahedra by four ligands each. The overall framework can be visualised as this smaller cubic net which is connected to a secondary identical net *via* the 12 corners of the cuboctahedra *via* Cu-N bonds. Thus, each ligand is a 3-connected node, with two isophthalate moieties that each connect an edge of a cuboctahedron, and one pyridyl N atom which joins a corner of a cuboctahedron. Figure shows views of a) structure of H_4L; b) the unit cell of MFM-170; c) the simplified structure showing the 'smaller' net of MFM-170; d) full structure resulting from connection of the two smaller nets; e) metal-ligand Cages *A*, *B* and *C*, observed in MFM-170.

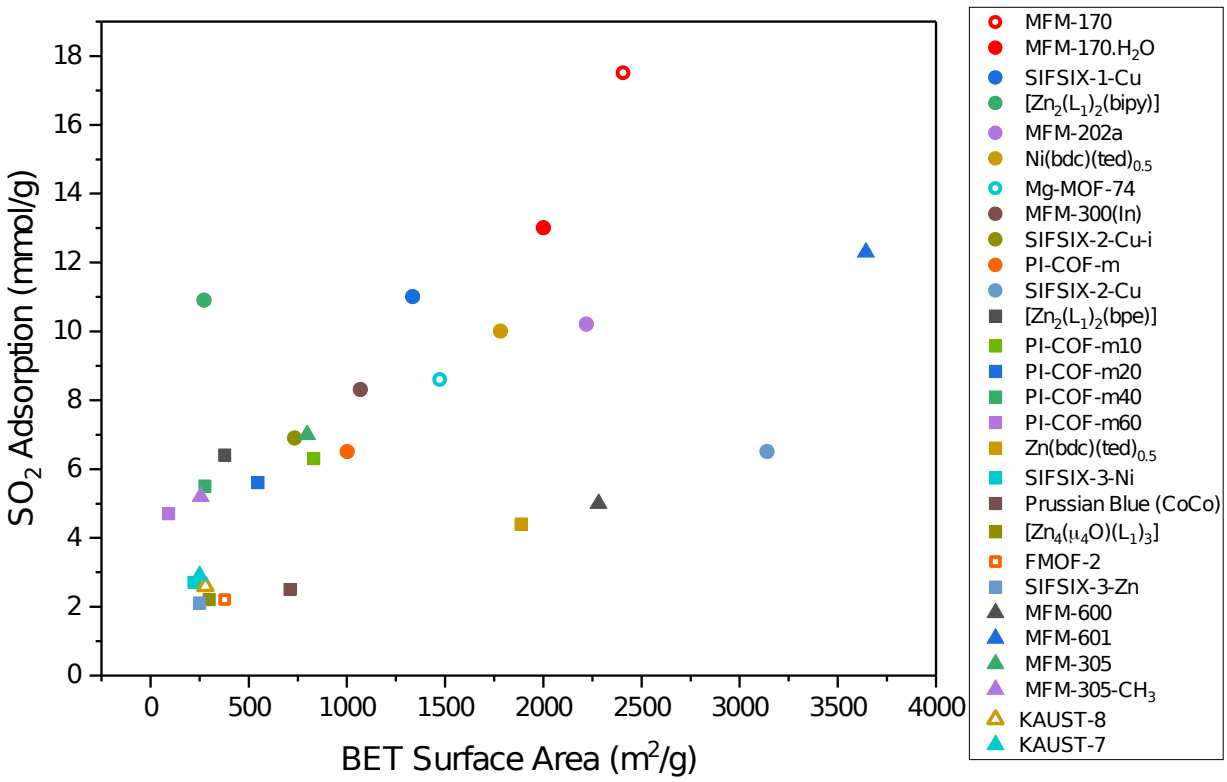

Fig. 2: Comparison of SO_2 uptakes of reported MOFs and COFs at 1.0 bar and 298 K. Plot of SO_2 adsorption (1.0 bar, 298 K) against BET surface area, where a general linear relationship between SO_2 uptake and BET surface area is observed . Open symbols denote the presence of open metal sites in the MOF structure.

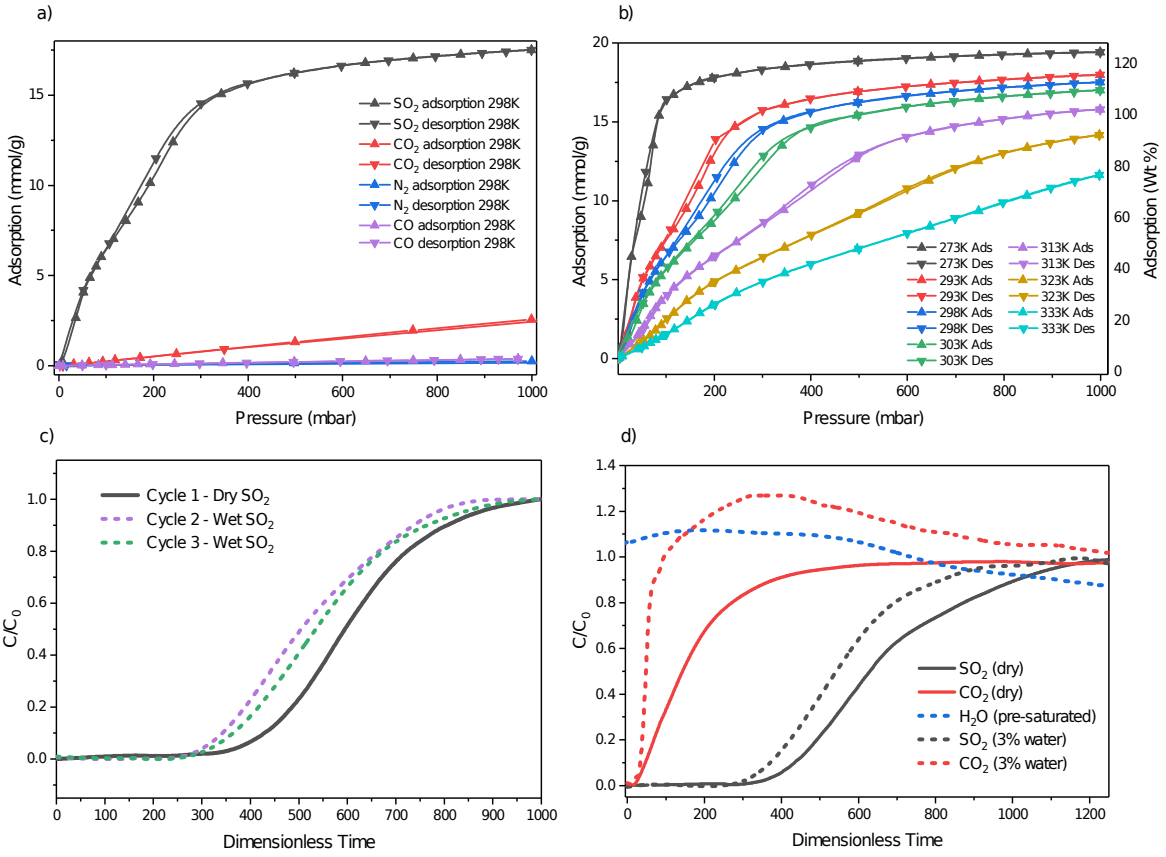
a)
Adsorption (mmol/g)
Pressure (mbar)
SO2 adsorption 298K
SO2 desorption 298K
CO2 adsorption 298K
CO2 desorption 298K
N2 adsorption 298K
N2 desorption 298K
CO adsorption 298K
CO desorption 298K
b)
Adsorption (mmol/g)
Adsorption (Wt %)
Pressure (mbar)
273K Ads
273K Des
293K Ads
293K Des
298K Ads
298K Des
303K Ads
303K Des
313K Ads
313K Des
323K Ads
323K Des
333K Ads
333K Des
c)
C/C0
Dimensionless Time
Cycle 1 - Dry SO2
Cycle 2 - Wet SO2
Cycle 3 - Wet SO2
d)
C/C0
Dimensionless Time
SO2 (dry)
CO2 (dry)
H2O (pre-saturated)
SO2 (3% water)
CO2 (3% water)

Fig. 3: Gas sorption and separation properties of MFM-170. a) adsorption and desorption isotherms for MFM-170 at 298 K up to 1 bar for SO_2 (black), CO_2 (red), N_2 (blue) and CO (purple). At 298 K and 1.0 bar, the volumetric storage density of SO_2 in MFM-170 is 307 times that of gaseous SO_2 under the same conditions, or 75 times of that of compressed SO_2 (P_0 = 3.9 bar) in a pressure vessel (packing efficiency and system volume are not taken into consideration); b) SO_2 adsorption and desorption isotherms for MFM-170 at 273-333 K up to 1 bar. Wt % is in terms of SO_2(g)/MOF(g). c) Breakthrough curves for SO_2 at 298 K under dry (solid line) and humid (dashed lines) conditions. The consistency in the retention time for SO_2 under humid conditions confirms the high stability of MFM-170. Dry conditions: 99.75% He, 2500 ppm SO_2; Wet Conditions: 98.25% He, 1.5% H_2O, 2500 ppm SO_2. Flow rate 26 mL min^{-1}. d) Comparison of the binary SO_2/CO_2 dynamic separations at 298 K under dry (solid line) and humid (dashed line) conditions. The dry sample was first activated under a flow of He at 423 K and the subsequent gas mixture composition was 84.75% He, 15% CO_2 and 2500 ppm SO_2 at a total flow rate of 26 mL min^{-1}. For experiments under humid conditions, the bed was first exposed to a flow of 3% H_2O in He until breakthrough of water (not shown). The subsequent gas mixture composition was ~81.6% He, 18% CO_2 and 4050 ppm SO_2 with a total flow rate of 16 mL min^{-1}.. Due to the experimental set-up, He was used instead of N_2 as a non-interacting component. Dimensionless time, τ, is equal to $tu/\varepsilon L$, where t is the actual breakthrough time, u is the gas velocity, ε is the fractional porosity and L is the length of the fixed bed. See SI for details.

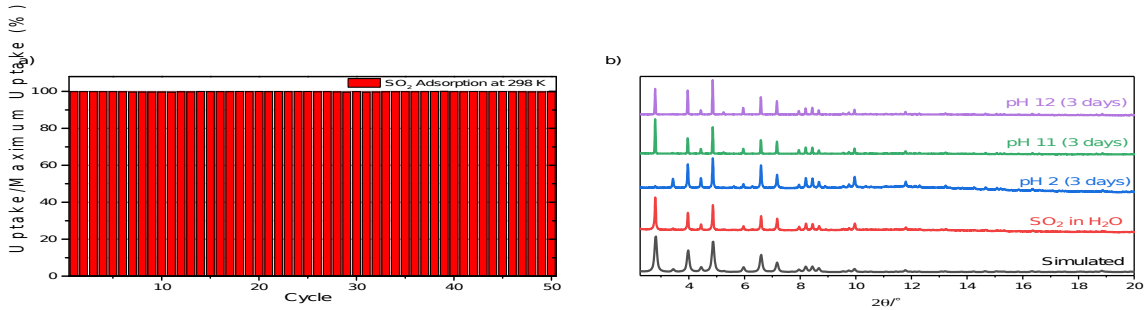

Fig. 4. Chemical stability tests for MFM-170. a) 50 adsorption-desorption cycles for SO_2 in MFM-170 at 298 K. All SO_2 is fully desorbed under vacuum at 298 K between cycles. No loss of uptake capacity is observed. b) PXRD analysis of MFM-170 exposed to various external conditions. Changes of intensities of Bragg peaks correspond to the inclusion of guest species in the pores of MFM-170. Pawley refinements are shown in the Supplementary Information.

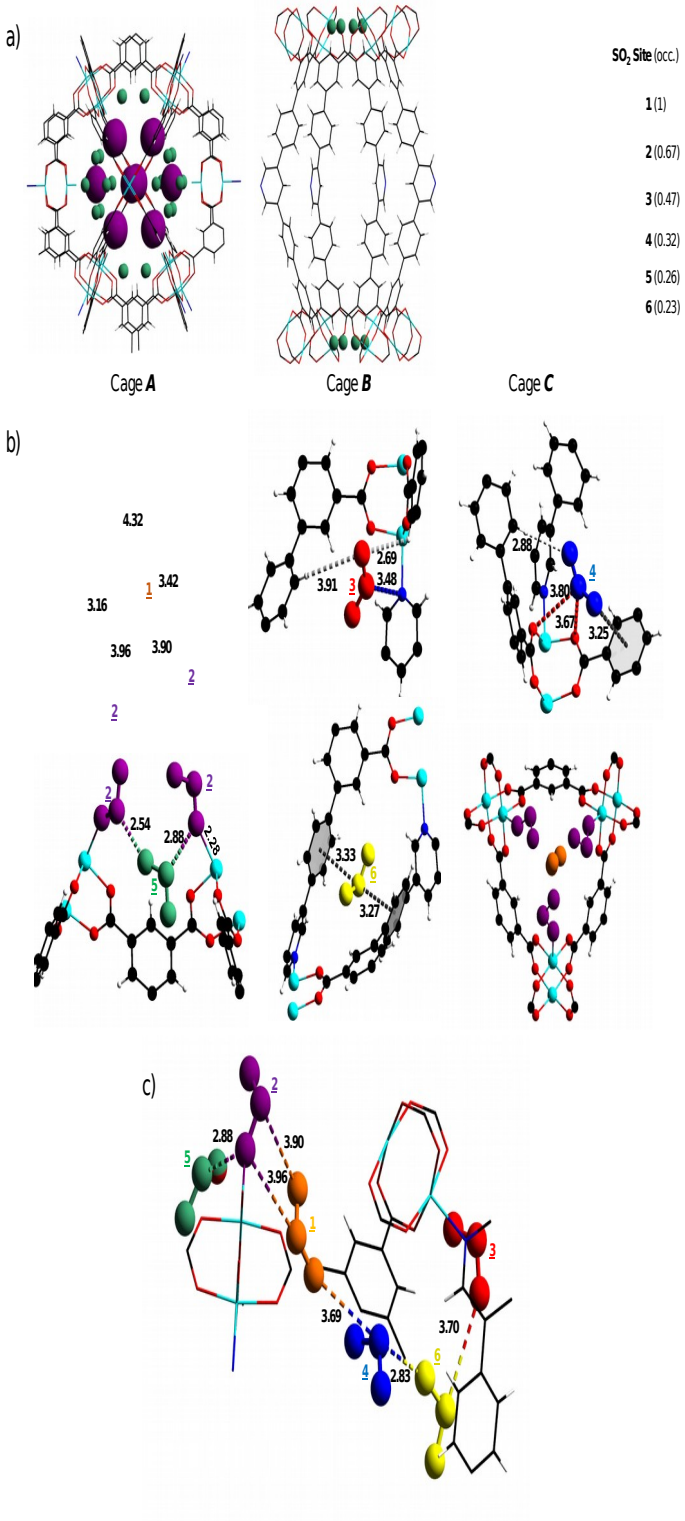

Fig. 5: Positions of SO_2 molecules located within the pores of MFM-170·5.46SO_2 from *in situ* single crystal XRD. a) Packing of SO_2 with in cages ***A, B*** and ***C***. The smallest cage ***C*** accounts for ~45% of all located SO_2 molecules, whilst ~25% is found in the cuboctahedral cage ***A***. No ordered SO_2 molecules were located in the largest cage ***B***, reflecting the large void space and lack of functional groups lining the pore. Size of the coloured balls depicting sites **1-6** are proportional to their occupancy. Site **3** is found in a crevice between two perpendicular cage ***B*** and are therefore not shown in the cages. b) Site (colour, occupancy): **1** (orange, 1.00); **2** (purple, 0.670); **3** (red, 0.468); **4** (blue 0.316); **5** (green, 0.262); and **6** (yellow, 0.233). c) Intermolecular interactions between adsorbed SO_2 molecules. SO_2 molecules have been magnified slightly for clarity. Distances are in Å.

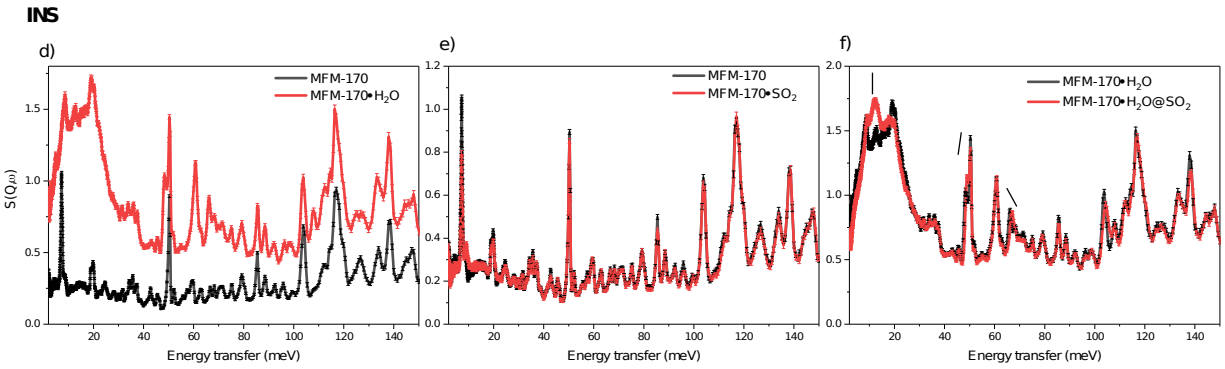

Fig 6. *In situ* vibrational spectra of MFM-170. a-c) FT-IR spectra of MFM-170 at various SO_2 loadings up to 0.50 ppSO_2. a) Redshift of carboxylate ν_{as}(COO) stretching mode at 1658 cm^{-1} and pyridine ring vibrational band ν(CC/CN) at 1595 cm^{-1}; b) Red shift of ν_s(COO) stretching mode at 1470 cm^{-1} and the ν_3 asymmetric stretch of adsorbed SO_2; c) growth of a new band at 1143 cm^{-1} assigned to the ν_1 symmetric stretch of adsorbed SO_2. All FT-IR spectra were collected at 1.0 bar, using N_2 as a balancing gas. The fundamental ν_3 antisymmetric stretch of gas phase SO_2 at 1361 cm^{-1} saturates at low partial pressures in this experiment (Fig. S21), and therefore the region of 1400-1300 cm^{-1} was only monitored up to 0.10 ppSO_2; d-f) INS spectra of MFM-170: d) Activated MFM-170 and MFM-170•H_2O. Additional peaks in MFM-170•H_2O are attributed to vibrational modes of water molecules: translational mode at 30 meV, rocking mode at 48 meV and wagging and twisting modes at 61 and 66 meV; e) Activated MFM-170 and MFM-170@SO_2. Minimal difference is observed between the two spectra; f) MFM-170•H_2O and MFM-170•H_2O@SO_2. Shifts in water modes are observed indicating $H_2O\cdots SO_2$ interactions.